C-section and systemic inflammation synergize to disrupt the neonatal gut microbiota and brain development in a model of prematurity

Cécile Morin, Flora Faure, Julie Mollet, David Guenoun, Ariane Heydari-Olya, Irvin Sautet, Sihao Diao, Valérie Faivre, Julien Pansiot, Lara Tabet, et al.

Brain, Behavior, and Immunity 123 (2025) 824–837

Contents lists available at ScienceDirect

Brain Behavior and Immunity

journal homepage: www.elsevier.com/locate/ybrbi

C-section and systemic inflammation synergize to disrupt the neonatal gut microbiota and brain development in a model of prematurity

Cécile Morin [a,b,1], Flora Faure [c,1], Julie Mollet [a,1], David Guenoun [a,d], Ariane Heydari-Olya [a], Irvin Sautet [a], Sihao Diao [a,e], Valérie Faivre [a], Julien Pansiot [a], Lara Tabet [a], Jennifer Hua [a], Leslie Schwendimann [a], Amazigh Mokhtari [a], Rebeca Martin-Rosique [f], Sead Chadi [f], Mireille Laforge [a], Charlie Demené [c], Andrée Delahaye-Duriez [a,g,h], Rochellys Diaz-Heijtz [i], Bobbi Fleiss [j], Boris Matrot [a], Sandrine Auger [f], Mickael Tanter [c], Juliette Van Steenwinckel [a,1], Pierre Gressens [a,1], Cindy Bokobza [a,*,1]

[a] Université Paris Cité, Inserm, NeuroDiderot, F-75019 Paris, France
[b] Department of Obstetrics and Gynecology, AP-HP, Robert Debré Hospital, 75019 Paris, France
[c] Physics for Medicine Paris, Inserm, ESPCI Paris-PSL, CNRS, 75015 Paris, France
[d] Department of Pharmacy, AP-HP, Robert Debré Hospital, 75019 Paris, France
[e] Fudan University, Department of Neonatology, Children's Hospital of Fudan University, 201102 Shanghai, China
[f] INRAE, Université Paris-Saclay, AgroParisTech, UMR1319 Micalis Institute, 78352 Jouy-en-Josas, France
[g] UFR Santé Médecine et Biologie Humaine, Université Sorbonne Paris Nord, 93000 Bobigny, France
[h] Unité Fonctionnelle de Médecine Génomique et Génétique Clinique, Hôpital Jean Verdier, Hôpitaux Universitaires Paris Seine Saint-Denis, Assistance Publique des Hôpitaux de Paris, 93140 Bondy, France
[i] Department of Neuroscience, Karolinska Institutet, 171 77 Stockholm, Sweden
[j] School of Health and Biomedical Sciences, STEM College, RMIT University, Bundoora, Melbourne, Victoria 3083, Australia

ARTICLE INFO

Keywords:
Neurodevelopmental disorders
Microglia
Myelination
Social interactions

ABSTRACT

Infants born very preterm (below 28 weeks of gestation) are at high risk of developing neurodevelopmental disorders, such as intellectual deficiency, autism spectrum disorders, and attention deficit. Preterm birth often occurs in the context of perinatal systemic inflammation due to chorioamnionitis and postnatal sepsis. In addition, C-section is often performed for very preterm neonates to avoid hypoxia during a vaginal delivery. We have developed and characterized a mouse model based on intraperitoneal injections of IL-1β between postnatal days one and five to reproduce perinatal systemic inflammation. This model replicates several neuropathological, brain imaging, and behavioral deficits observed in preterm infants. We hypothesized that C-sections could synergize with systemic inflammation to induce more severe brain abnormalities. We observed that C-sections significantly exacerbated the deleterious effects of IL-1β on reduced gut microbial diversity, increased levels of circulating peptidoglycans, abnormal microglia/macrophage reactivity, impaired myelination, and reduced functional connectivity in the brain relative to vaginal delivery plus intraperitoneal saline. These data demonstrate the deleterious synergistic effects of C-section and neonatal systemic inflammation on brain maldevelopment and malfunction, two conditions frequently observed in very preterm infants, who are at high risk of developing neurodevelopmental disorders.

1. Introduction

Preterm delivery (WHO definition: below 38 weeks of gestation) occurs in more than 10 % of births worldwide and is associated with a very significant increased risk of motor deficits (cerebral palsy), intellectual deficiency, and psychiatric disorders (including autism spectrum disorder and attention deficit) relative to term delivery (Chevallier, 2022; Twilhaar, 2022; O'Reilly, 2021).

* Corresponding author at: Inserm Unité 1141, Hôpital Robert Debré 48 Boulevard Sérurier, 75019 Paris, France.
E-mail address: cindy.bokobza@inserm.fr (C. Bokobza).
[1] Equal contribution.

https://doi.org/10.1016/j.bbi.2024.10.023
Received 31 October 2023; Received in revised form 7 October 2024; Accepted 20 October 2024
Available online 22 October 2024

Imaging and post-mortem studies of preterm infants combined with experimental models have identified the brain abnormalities associated with a poor long-term neurological prognosis. These abnormalities, grouped under the term encephalopathy of prematurity (EoP), include diffuse white matter injury related to delayed myelination induced by the blockade of maturation of oligodendrocyte progenitor cells (OPCs), microglia and astrocyte activation, which play a pivotal role in the pathogenic cascade, a reduction in the density of subsets of interneurons, the abnormal microstructure of cortical grey matter, and reduced brain connectivity (Stolp, 2019; Verney, 2010; Vogel, 2015; Ball, 2013; Ball, 2015; Buser, 2012).

Epidemiological and clinical studies have highlighted an important role for sustained systemic inflammation in the etiology of EoP (Leviton and Dammann, 2004). Several conditions can contribute to perinatal inflammation in preterm infants, including prenatal chorioamnionitis, postnatal sepsis, mechanical ventilation, and delayed necrotizing enterocolitis (Nadeau et al., 2016; Bennet, 2018).

Gut microbiota dysbiosis has been shown to be associated with several neurodevelopmental disorders (NDDs), including autism spectrum disorder, although its pathogenic role is still a subject of debate (Iglesias-Vazquez, 2020; Zuffa, 2023; Thion, 2018; Shiow, 2017). In the context of preterm delivery, several studies have reported a reduced diversity of gut microbiota that can persist for several weeks or months after birth (Dahl, 2018; Koenig, 2011; Underwood and Sohn, 2017; Korpela, 2018; Rao, 2021). Several factors have been shown to potentially induce or be associated with dysbiosis in preterm infants, including cesarean delivery (C-section), preventing colonization by the vaginal microbiota, exposure to multiple rounds of broad-spectrum antibiotics, sustained systemic inflammation, and delayed introduction of oral feeding (Backhed, 2015; Cryan, 2019; Curran, 2015; Xiao, 2021).

C-sections are often performed for very preterm neonates to avoid the hypoxia that occurs during vaginal delivery. However, several epidemiological studies have shown an association between C-sections and NDDs (Curran, 2015; Yip, 2017; Thanh, 2019). Based on the evidence cited above, this raises the question of potential deleterious interactions between C-section and sustained systemic inflammation in the genesis of the EoP and whether these two factors act independently or synergize to worsen the dysbiosis and associated brain maldevelopment that lead to NDDs.

We have developed a rodent model of EoP based on the neonatal intraperitoneal injection of the inflammatory cytokine IL-1β from postnatal day (P) 1 to P5, during a developmental stage of the mouse brain that corresponds to a window of vulnerability for human preterm birth (23–32 weeks' gestation) (Hagberg et al., 2002). This model recapitulates several key hallmarks of human EoP including systemic inflammation (Bokobza, 2022; Favrais, 2011), prematurity (Morin, 2022), microglial activation (Bokobza, 2022; Krishnan, 2017; Van Steenwinckel, 2019), oligodendrocyte delayed maturation (Favrais, 2011; Morin, 2022; Van Steenwinckel, 2019), astrocyte activation (Shiow, 2017; Bokobza, 2022), interneuron loss (Stolp, 2019), decreased functional connectivity, cognitive and social behaviour impairments (Favrais, 2011; Bokobza, 2022; Van Steenwinckel, 2019; Veerasammy, 2020), and sex difference (Rangon, 2018). We have used this model to show that pro-inflammatory activation of microglia/macrophages induced by IL-1β is a major event that leads to the blockade of OPC maturation and the subsequent delay in myelination (Bokobza, 2022; Van Steenwinckel, 2019).

Here, we used this EoP model to combine C-section and neonatal systemic inflammation (IL-1β) and determine the impact of each factor or their combination on the gut microbiota, microglia activation, myelination, brain connectivity, and behaviour (Fig. 1A) relative to the control condition of vaginal delivery (V-delivery) and neonatal systemic saline (PBS).

2. Results

2.1. Impact of C-section and systemic inflammation on the gut microbiota and peptidoglycan levels

We studied the composition of the gut microbiota at P5 from colon samples to determine whether C-section and systemic inflammation influence this microbiota. Amplicon sequencing of bacterial 16S-rRNA generated operational taxonomic units (OTUs). Firmicutes, including the genera Lactobacillus, Streptococcus, Enterococcus, and Staphylococcus, was the predominant phylum in the four mouse groups, followed by Proteobacteria and Bacteroidota (Fig. 1B, Supplementary Fig. 1). We used hierarchical clustering analysis to group the OTUs according to their relative abundance within the four groups (Table 1). The effect of C-section and IL-1β-exposure on the abundance of various OTUs was evident, and they were divided into six clusters (A to F) (Fig. 1C). The abundance of the OTUs corresponding to the Lactobacillus genera was highly heterogeneous between groups. Certain Lactobacillus OTUs were found to be over-represented in clusters A and B and under-represented in clusters C and F (Fig. 1C). In addition, cluster F showed the proliferation of Streptococcus and Enterococcus OTUs in the V-delivery + PBS group, whereas these species were less abundant in the other groups, even disappearing in the C-section + IL-1β group (Fig. 1C, Supp. Fig. 1A). Furthermore, OTUs associated with Proteobacteria, specifically those relevant to Escherichia-Shigella in cluster A, were more abundant only in the C-section + PBS group (Fig. 1C, Supplementary Fig. 1B). Finally, IL-1β-exposure specifically promoted over-representation of OTUs, such as Corynebacterium and Desulfovibrionaceae (Cluster B), which could be modulated by C-section, as seen with Cloacibacterium and Diaphorobacter in cluster D (Fig. 1C).

We further evaluated the α-diversity of the gut microbiota using various indexes. The observed species and Chao1 index were used to determine the number of species present, while the Shannon and InvSimpson indexes assessed the variety and evenness of the species (McMurdie and Holmes, 2013). The C-section + IL-1β group showed a significant decrease in observed diversity ($p = 0.017$). In addition, we observed a significant decrease in the Shannon and InvSimpson indexes in the C-section + PBS group ($p = 0.04$). This effect was even more pronounced in the C-section + IL-1β group ($p < 0.0001$) relative to the V-delivery + PBS group (Fig. 1D). In adults, the alteration in microbiota diversity is largely, but not completely, restored (Supp. Fig. 2).

Peptidoglycan (PGN) motifs derived from commensal gut microbiota can be translocated into the developing brain and sensed by specific pattern recognition receptors (PRRs) of the innate immune system (Arentsen, 2017; Tosoni et al., 2019). We evaluated PGN levels in the plasma and brain at P5 (Wu, 2022; Beli, 2018). Plasma PGN levels in the C-section + IL-1β group were significantly higher than those in the V-delivery + PBS group ($p = 0.039$) (Fig. 1E). By contrast, brain PGN levels in the V-delivery + IL-1β group were significantly lower than those in the V-delivery + PBS group ($p = 0.046$) (Fig. 1F). This reduction in brain PGN levels could be linked to the significant under-expression ($p = 0.036$) of brain *Pept1* mRNA, one of the PGN transporters within the brain, in the V-delivery + IL-1β group (Fig. 1G).

PGNs interact with two families of specific pattern recognition receptors (PRRs): PGN-recognition proteins (PGLYRP1-4) and NOD-like receptors (NOD1-2) (Royet et al., 2011; Arentsen, 2018). In a previous study, we performed transcriptomic analysis (mRNA microarrays) of $CD11B^+$ brain cells from V-delivery + PBS and V-delivery + IL-1β groups using the same model of EoP. These data showed higher *Nod1-2 and Tlr2* and only *Pglyrp1* mRNA expression in $CD11B^+$ microglia/macrophages in the V-delivery + IL-1β group (Supp. Fig. 3). Here, we extended this analysis to the four studied groups by qRT-PCR analysis of $CD11B^+$ cells (Fig. 1H). We confirmed the significant overexpression of *Nod2* ($p = 0.004$), *Pglyrp1* ($p = 0.004$), and *Tlr2* ($p = 0.003$) mRNA in the V-delivery + IL-1β group and observed comparable overexpression of these three mRNAs the C-section + IL-1β group ($p = 0.024$, 0.047, and 0.006,

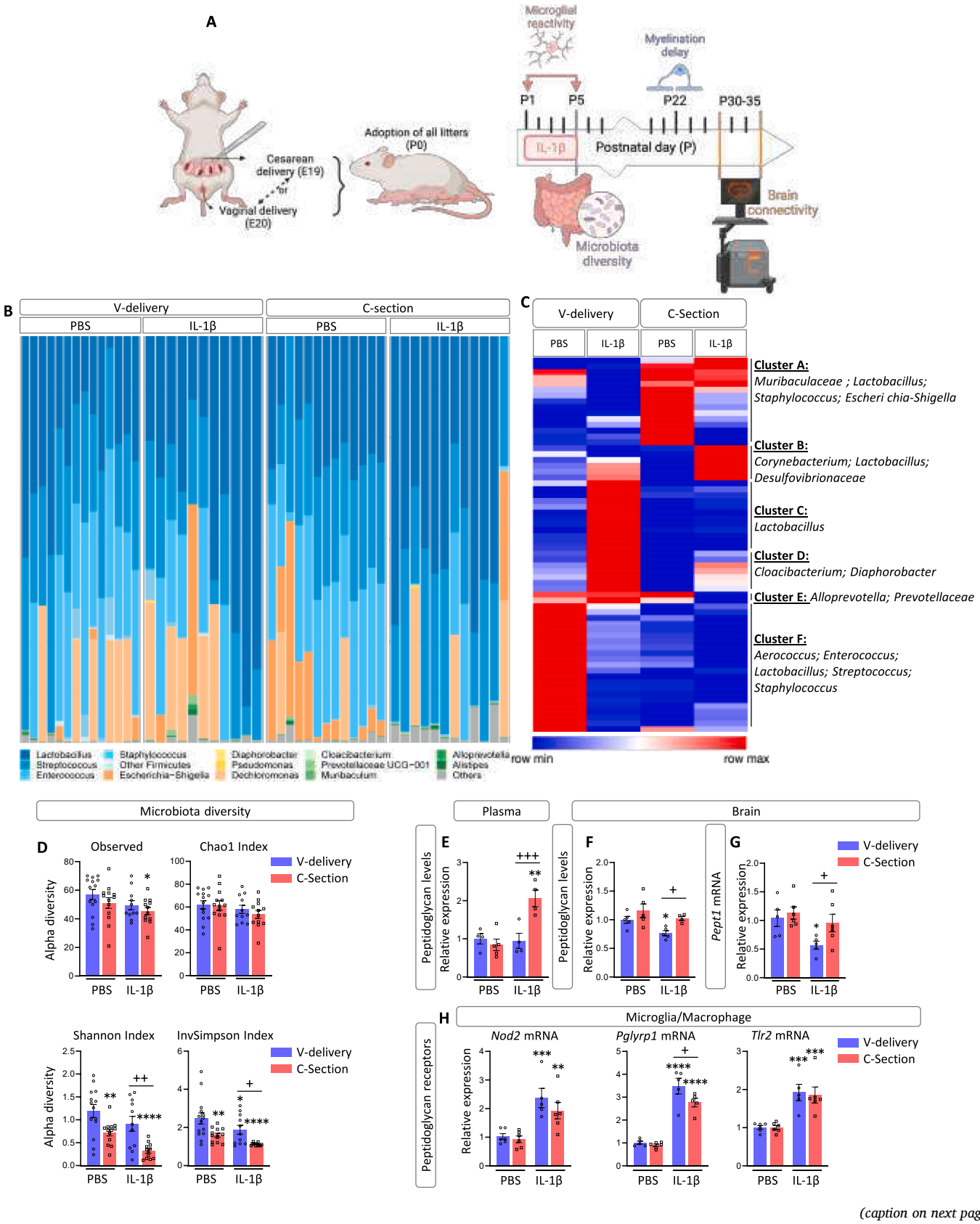

(caption on next page)

Fig. 1. Impact of IL-1β and C-section on microbiota composition and peptidoglycan release. (A) Schematic representation of the experimental protocol. (B) Table of abundance of operational taxonomic units (OTUs). Analysis of the individual distribution of the genera that make up the intestinal microbiota at P5 in V-delivery ± IL-1β or C-section ± IL-1β mice. Each phylum is represented by a different color. (C) Heatmap representation of the differential analysis of the OTUs (BH $p < 0.05$) by hierarchical clustering using Pearson's correlation. (D) Diversity of the intestinal microbiota at P5 depending on the delivery route and the presence or absence of systemic inflammation. Alpha diversity was determined using the following four indexes: Observed, Chao1, Shannon, and InvSimpson. n = 12–14 per group, 2 litters per group. (E-F) Relative expression of peptidoglycan levels in the plasma (E) and brain (F) at P5 of V-delivery ± IL-1β or C-section ± IL-1β mice, n = 4–5 per group, 1 litter per group. (G) Relative expression of *Pept1* mRNA at P5 in the anterior brain of V-delivery ± IL-1β or C-section ± IL-1β mice, n = 4–5 per group, 2 litters per group. (H) Relative expression of microglial peptidoglycan receptor mRNA at P5 in CD11B + cells of V-delivery ± IL-1β or C-section ± IL-1β mice, n = 5–6 per group, 2 litters per group. Data are presented as a scatter plot with a bar (mean + SEM). The Kruskal-Wallis Test was used followed by an uncorrected Dunn's test. All groups were compared to the V-delivery + PBS group, indicated by *.

respectively).

2.2. Impact of C-section and systemic inflammation on microglial activation

We previously showed that $CD11B^+$ microglia/macrophages in the V-delivery + IL-1β group overexpress pro-inflammatory markers as soon as two hours after the first IL-1β injection relative to the V-delivery + PBS group (Krishnan, 2017; Van Steenwinckel, 2019). Here, we extended this analysis to the four studied groups by qRT-PCR quantification of several markers of microglia/macrophage reactivity on $CD11B^+$ cells (Fig. 2A-H). We confirmed the significant overexpression at P1 of *prostaglandin-endoperoxide synthase 2 (Ptgs2*, a pro-inflammatory factor*), tumor necrosis factor* (*Tnf,* a pro-inflammatory factor*), and interleukin 1 receptor antagonist (Il1ra*, an immunomodulatory factor) mRNA ($p = 0.0001$, 0.008, and 0.0001, respectively) combined with a delayed increase at P5 of *Arg1* (*arginase 1*, an anti-inflammatory factor) mRNA expression ($p = 0.03$) in the V-delivery + IL-1β group relative to the V-delivery + PBS group. We did not observe any significant difference in mRNA expression between the C-section + PBS and V-delivery + PBS groups. By contrast, at P1, there was very robust induction of *cluster of differentiation 32, (Cd32, a pro-inflammatory factor*), *Ptgs2, Tnf, Il1ra*, and *interleukin 4 receptor antagonist*, (*Il-4ra,* an immunomodulatory factor) mRNA expression ($p < 0.0001$) along with a delayed increase at P5 of *Arg1* mRNA expression ($p < 0.0001$) in the C-section + IL-1β group relative to the V-delivery + PBS group. The overexpression of *Cd32*, *Il1ra*, *Il-4ra* and *Tnf* mRNAs was significantly more robust in the C-section + IL-1β group than in the V-delivery + IL-1β group. We further characterized the microglial/macrophage profile by analyzing the release of reactive oxygen species (ROS) by $CD11B^+$ cells sorted at P1 and P5. ROS were measured under basal conditions and after PMA stimulation of sorted $CD11B^+$ cells (Fig. 2G) (Bokobza, 2022; Bokobza, 2022). Under basal conditions, we did not observe any ROS release from P1 $CD11B^+$ cells in any experimental group, whereas P5 $CD11B^+$ cells sorted from the V-delivery + IL-1β and C-section + IL-1β groups produced a significantly higher amount of ROS ($p < 0.0001$) than those from the V-delivery + PBS group. Under PMA stimulation, P1 $CD11B^+$ cells sorted from the C-section + IL-1β group produced a significantly higher amount of ROS ($p = 0.011$) than those of the V-delivery + PBS group. The data for sorted $CD11B^+$ cells at P5 under PMA stimulation and basal conditions were comparable. Microglial activation occurs at different levels over time. At P1, the changes are primarily observed at the mRNA expression level. By P5, these changes are more pronounced at the protein level, as evidenced by the significantly higher basal ROS production at P5 compared to P1. This suggests a dynamic shift in microglial activation from transcriptional to functional responses over this period.

We further characterized the microglia and infiltrating macrophages in the present model using a previously published gating strategy (Morin, 2022) by quantifying the microglia, defined as $CD11B^+CD45^{low}$ cells, and infiltrating macrophages, defined as $CD11B^+CD45^{high}$ cells, at P5 (Fig. 2H). In addition, we also measured the CD11B and CD18 mean fluorescence intensities (MFIs), used as markers of microglia/macrophage activation, at P5 (Fig. 2H). There was a significantly higher proportion of infiltrating $CD11B^+CD45^{high}$ cells in the V-delivery + IL-1β group than the V-delivery + PBS group (0.56 ± 0.1 % and 0.08 ± 0.004 %, respectively, $p = 0.0022$). There was a similar increase in the proportion of infiltrating macrophages in the C-section + IL-1β group (0.62 ± 0.1 % and 0.08 ± 0.004 %, $p = 0.0002$) relative to the V-delivery + PBS group. The infiltrating macrophages showed a significantly higher CD11B MFI in both the V-delivery + IL-1β and C-section + IL-1β groups than the V-delivery + PBS group ($p < 0.001$). There was a significantly higher proportion of infiltrating neutrophils ($CD11B^+Ly6C^+LY6G^+$) and monocytes ($CD11B^+Ly6C^+LY6G^-$) in IL-1β groups than in the V-delivery + PBS group (Supplementary Fig. 4). We did not observe any modulation in the percentage of $CD11B^+CD45^{low}$ cells in either the V-delivery + IL-1β or C-section + IL-1β groups relative to the V-delivery + PBS group; but we observed a significant decrease of $CD11B^+P2RY12^+$ cells in all groups relative to the V-delivery + PBS group (Supplementary Fig. 4, $p < 0.001$). However, the microglia showed a significantly higher CD11B MFI in the V-delivery + IL-1β and C-section + IL-1β groups than the V-delivery + PBS group ($p = 0.0005$ and $p < 0.0001$, respectively). This effect was significantly enhanced in the C-section + IL-1β group relative to the V-delivery + IL-1β group ($p = 0.0279$). In addition, the microglia showed a significantly higher CD18 MFI in the V-delivery + IL-1β and C-section + IL-1β groups than the V-delivery + PBS group ($p < 0.0001$ and $p = 0.014$). This effect was significantly less in the C-section + IL-1β group than the V-delivery + IL-1β group ($p = 0.0177$). We also measured the percentage of Boarder Associated Macrophages (BAM, $CD11B^+P2RY12^+CD206^+$ cells) and observed a significant decrease of this population in C-section + IL-1β group relative to the V-delivery + IL-1β group ($p = 0.0078$). Looking at systemic response, we analyzed cytokine/chemokine expression and blood cell phenotyping by FACS at P5. In response to systemic inflammation, we observed an increased proportion of granulocytes and a significant decrease of inflammatory monocytes in IL-1β-treated mice (Supplementary Fig. 5), likely due to monocyte infiltration into the inflamed brain (Supplementary Fig. 4), supported by elevated chemokine levels and consistent with increased brain macrophage infiltration (Fig. 2H).

2.3. Impact of C-section and systemic inflammation on the oligodendrocyte lineage and myelination

We next quantified the $PDGFR\alpha^+$, $PDGFR\alpha^+/O4^+$, and $O4^+$ cell populations by FACS (Morin, 2022) at P5 (Fig. 3A-B). There were significantly fewer $PDGFR\alpha^+$ and $PDGFR\alpha^+/O4^+$ cells ($p = 0.004$ and 0.001, respectively) in the V-delivery + IL-1β group than the V-delivery + PBS group. There was also a significant and comparable decrease in the number of $O4^+$ cells ($p < 0.001$) in the V-delivery + IL-1β and C-section + IL-1β groups. However, the $PDGFR\alpha^+/O4^+$ population was significantly smaller in the C-section + IL-1β ($p = 0.001$), whereas it was not in the V-delivery + IL-1β group. Using immunohistochemistry, we quantified the number of oligodendrocyte transcription factor (OLIG)-2^+ cells at P5 to assess the entire oligodendrocyte lineage (Fig. 3C). The number of OLIG-2^+ cells in the C-section + IL-1β group was significantly smaller ($p = 0.029$, Fig. 3D).

We then characterized myelination by quantifying the mRNA expression of three myelin proteins in the P22 forebrain by qRT-PCR (Fig. 3E). The expression of *myelin associated oligodendrocyte basic protein (Mobp), proteolipid protein 1 (Plp), and myelin basic protein (Mbp)*

Table 1
Heatmap clusters annotation.

Cluster A	
Cluster_27	Bacteria;Bacteroidota;Bacteroidia;Bacteroidales;Muribaculaceae; unknown genus;unknown species
Cluster_110	Bacteria;Bacteroidota;Bacteroidia;Bacteroidales;Muribaculaceae; unknown genus;unknown species
Cluster_117	Bacteria;Bacteroidota;Bacteroidia;Bacteroidales;Muribaculaceae; unknown genus;unknown species
Cluster_1	Bacteria;Firmicutes;Bacilli;Lactobacillales;Lactobacillaceae; Lactobacillus;Multi-affiliation
Cluster_141	Bacteria;Firmicutes;Bacilli;Lactobacillales;Lactobacillaceae; Lactobacillus;Multi-affiliation
Cluster_126	Bacteria;Firmicutes;Bacilli;Lactobacillales;Lactobacillaceae; Lactobacillus;Multi-affiliation
Cluster_135	Bacteria;Firmicutes;Bacilli;Lactobacillales;Lactobacillaceae; Lactobacillus;Multi-affiliation
Cluster_36	Bacteria;Firmicutes;Bacilli;Lactobacillales;Lactobacillaceae; Lactobacillus;Multi-affiliation
Cluster_72	Bacteria;Firmicutes;Bacilli;Lactobacillales;Lactobacillaceae; Lactobacillus;Multi-affiliation
Cluster_94	Bacteria;Firmicutes;Bacilli;Lactobacillales;Lactobacillaceae; Lactobacillus;Multi-affiliation
Cluster_198	Bacteria;Firmicutes;Bacilli;Lactobacillales;Lactobacillaceae; Lactobacillus;unknown species
Cluster_21	Bacteria;Firmicutes;Bacilli;Staphylococcales;Staphylococcaceae; Staphylococcus;Multi-affiliation
Cluster_165	Bacteria;Firmicutes;Bacilli;Staphylococcales;Staphylococcaceae; Staphylococcus;Multi-affiliation
Cluster_115	Bacteria;Proteobacteria;Gammaproteobacteria;Enterobacterales; Enterobacteriaceae;Escherichia-Shigella;Multi-affiliation
Cluster_2	Bacteria;Proteobacteria;Gammaproteobacteria;Enterobacterales; Enterobacteriaceae;Escherichia-Shigella;Multi-affiliation
Cluster B	
Cluster_140	Bacteria;Actinobacteriota;Actinobacteria;Corynebacteriales; Corynebacteriaceae;Corynebacterium;unknown species
Cluster_128	Bacteria;Desulfobacterota;Desulfovibrionia;Desulfovibrionales; Desulfovibrionaceae;unknown genus;unknown species
Cluster_24	Bacteria;Firmicutes;Bacilli;Lactobacillales;Lactobacillaceae; Lactobacillus;unknown species
Cluster_119	None
Cluster_143	None
Cluster_99	None
Cluster C	
Cluster_122	Bacteria;Firmicutes;Bacilli;Lactobacillales;Lactobacillaceae; Lactobacillus;Multi-affiliation
Cluster_118	Bacteria;Firmicutes;Bacilli;Lactobacillales;Lactobacillaceae; Lactobacillus;Multi-affiliation
Cluster_11	Bacteria;Firmicutes;Bacilli;Lactobacillales;Lactobacillaceae; Lactobacillus;Multi-affiliation
Cluster_136	Bacteria;Firmicutes;Bacilli;Lactobacillales;Lactobacillaceae; Lactobacillus;Multi-affiliation
Cluster_43	Bacteria;Firmicutes;Bacilli;Lactobacillales;Lactobacillaceae; Lactobacillus;Multi-affiliation
Cluster_15	Bacteria;Firmicutes;Bacilli;Lactobacillales;Lactobacillaceae; Lactobacillus;Multi-affiliation
Cluster_4	Bacteria;Firmicutes;Bacilli;Lactobacillales;Lactobacillaceae; Lactobacillus;Multi-affiliation
Cluster_106	Bacteria;Firmicutes;Bacilli;Lactobacillales;Lactobacillaceae; Lactobacillus;unknown species
Cluster_138	Bacteria;Firmicutes;Bacilli;Lactobacillales;Lactobacillaceae; Lactobacillus;unknown species
Cluster_12	Bacteria;Firmicutes;Bacilli;Lactobacillales;Lactobacillaceae; Lactobacillus;unknown species
Cluster_35	Bacteria;Firmicutes;Bacilli;Lactobacillales;Lactobacillaceae; Lactobacillus;unknown species
Cluster_18	Bacteria;Firmicutes;Bacilli;Lactobacillales;Lactobacillaceae; Lactobacillus;unknown species
Cluster_34	None
Cluster_47	None
Cluster D	
Cluster_60	Bacteria;Bacteroidota;Bacteroidia;Flavobacteriales;Weeksellaceae; Cloacibacterium;Multi-affiliation
Cluster_30	Bacteria;Proteobacteria;Gammaproteobacteria;Burkholderiales; Comamonadaceae;Diaphorobacter;Multi-affiliation
Cluster_127	None
Cluster_81	None
Cluster_61	None
Cluster E	
Cluster_116	Bacteria;Bacteroidota;Bacteroidia;Bacteroidales;Prevotellaceae; Alloprevotella;unknown species
Cluster_85	Bacteria;Bacteroidota;Bacteroidia;Bacteroidales;Prevotellaceae; Prevotellaceae UCG-001;unknown species
Cluster F	
Cluster_32	Bacteria;Firmicutes;Bacilli;Lactobacillales;Aerococcaceae; Aerococcus;Multi-affiliation
Cluster_17	Bacteria;Firmicutes;Bacilli;Lactobacillales;Enterococcaceae; Enterococcus;Enterococcus faecalis
Cluster_5	Bacteria;Firmicutes;Bacilli;Lactobacillales;Enterococcaceae; Enterococcus;Multi-affiliation
Cluster_55	Bacteria;Firmicutes;Bacilli;Lactobacillales;Enterococcaceae; Enterococcus;Multi-affiliation
Cluster_8	Bacteria;Firmicutes;Bacilli;Lactobacillales;Enterococcaceae; Enterococcus;Multi-affiliation
Cluster_10	Bacteria;Firmicutes;Bacilli;Lactobacillales;Lactobacillaceae; Lactobacillus;Multi-affiliation
Cluster_20	Bacteria;Firmicutes;Bacilli;Lactobacillales;Lactobacillaceae; Lactobacillus;Multi-affiliation
Cluster_26	Bacteria;Firmicutes;Bacilli;Lactobacillales;Lactobacillaceae; Lactobacillus;Multi-affiliation
Cluster_29	Bacteria;Firmicutes;Bacilli;Lactobacillales;Lactobacillaceae; Lactobacillus;Multi-affiliation
Cluster_33	Bacteria;Firmicutes;Bacilli;Lactobacillales;Lactobacillaceae; Lactobacillus;Multi-affiliation
Cluster_37	Bacteria;Firmicutes;Bacilli;Lactobacillales;Lactobacillaceae; Lactobacillus;Multi-affiliation
Cluster_57	Bacteria;Firmicutes;Bacilli;Lactobacillales;Lactobacillaceae; Lactobacillus;Multi-affiliation
Cluster_87	Bacteria;Firmicutes;Bacilli;Lactobacillales;Lactobacillaceae; Lactobacillus;Multi-affiliation
Cluster_28	Bacteria;Firmicutes;Bacilli;Lactobacillales;Lactobacillaceae; Lactobacillus;unknown species
Cluster_44	Bacteria;Firmicutes;Bacilli;Lactobacillales;Lactobacillaceae; Lactobacillus;unknown species
Cluster_13	Bacteria;Firmicutes;Bacilli;Lactobacillales;Multi-affiliation;Multi-affiliation;Multi-affiliation
Cluster_3	Bacteria;Firmicutes;Bacilli;Lactobacillales;Streptococcaceae; Streptococcus;unknown species
Cluster_39	Bacteria;Firmicutes;Bacilli;Lactobacillales;Streptococcaceae; Streptococcus;unknown species
Cluster_45	Bacteria;Firmicutes;Bacilli;Lactobacillales;Streptococcaceae; Streptococcus;unknown species
Cluster_90	Bacteria;Firmicutes;Bacilli;Lactobacillales;Streptococcaceae; Streptococcus;unknown species
Cluster_102	Bacteria;Firmicutes;Bacilli;Staphylococcales;Staphylococcaceae; Staphylococcus;Multi-affiliation
Cluster_6	Bacteria;Firmicutes;Bacilli;Staphylococcales;Staphylococcaceae; Staphylococcus;Multi-affiliation

mRNA was significantly lower in the V-delivery + IL1β group ($p = 0.042$, 0.014, and 0.06, respectively) and even lower in the C-section + IL1β group ($p < 0.001$).

MBP is among the most abundant myelin proteins in the brain (Boggs, 2006). We previously demonstrated that western blotting evaluation of MBP in the forebrain is a simple and robust method to evaluate the hypomyelination observed in the V-delivery + IL-1β group relative to the V-delivery + PBS group (Van Steenwinckel, 2019; Bokobza, 2021). Here (Fig. 3F), we confirmed that MBP expression is significantly lower in the V-delivery + IL-1β group than the V-delivery + PBS group ($p = 0.019$) and showed such under-expression to be exacerbated in the C-section + IL-1β group ($p < 0.0001$).

Microglia/Macrophage reactivity

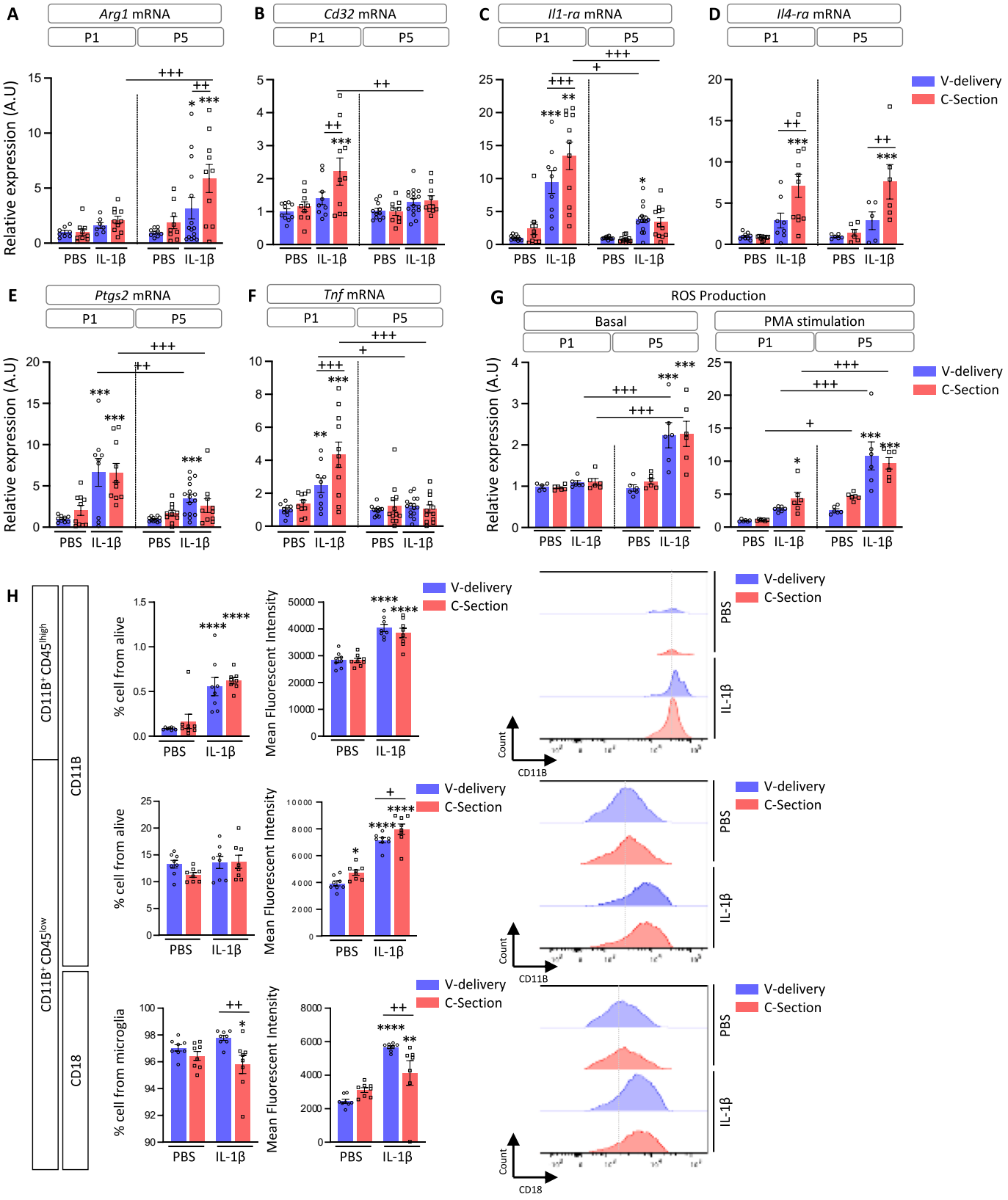

(caption on next page)

Fig. 2. Impact of IL-1β and C-section on microglial reactivity. (A-F) Relative expression of microglial reactivity markers (pro-inflammatory, immune-regulatory, and anti-inflammatory) evaluated by qPCR from CD11B^{+} cells from P1 and P5 brains from V-delivery ± IL-1β or C-section ± IL-1β mice. n = 6–9 per group, 2 litters per group. Comparisons between groups and ages were performed using two-way ANOVA followed by a post hoc uncorrected Fisher's LSD test. All groups were compared to the P1 V-delivery + PBS group. (G) ROS production from CD11B^{+} cells from P1 and P5 brains from V-delivery ± IL-1β or C-section ± IL-1β mice. n = 6–7 per group, 1 litter per group. Comparisons between groups and ages were performed using 2-way ANOVA followed by a post hoc uncorrected Fisher's LSD test. All groups were compared to the P1 V-delivery + PBS group, indicated by *. (H) Flow cytometry analysis of microglial reactivity in P5 brains from V-delivery ± IL-1β or C-section ± IL-1β mice, 1 litter per group. Macrophages were defined as CD11B+/CD45^{high}. Microglia were defined as CD11B+/CD45^{low}. The proportion of microglia and the expression of CD11B and CD18 were evaluated. Data are represented as a scatter plot with a bar (mean + SEM). The Kruskal-Wallis Test was used followed by an uncorrected Dunn's test, n = 8 per group. All groups were compared to the V-delivery + PBS group, indicated by *.

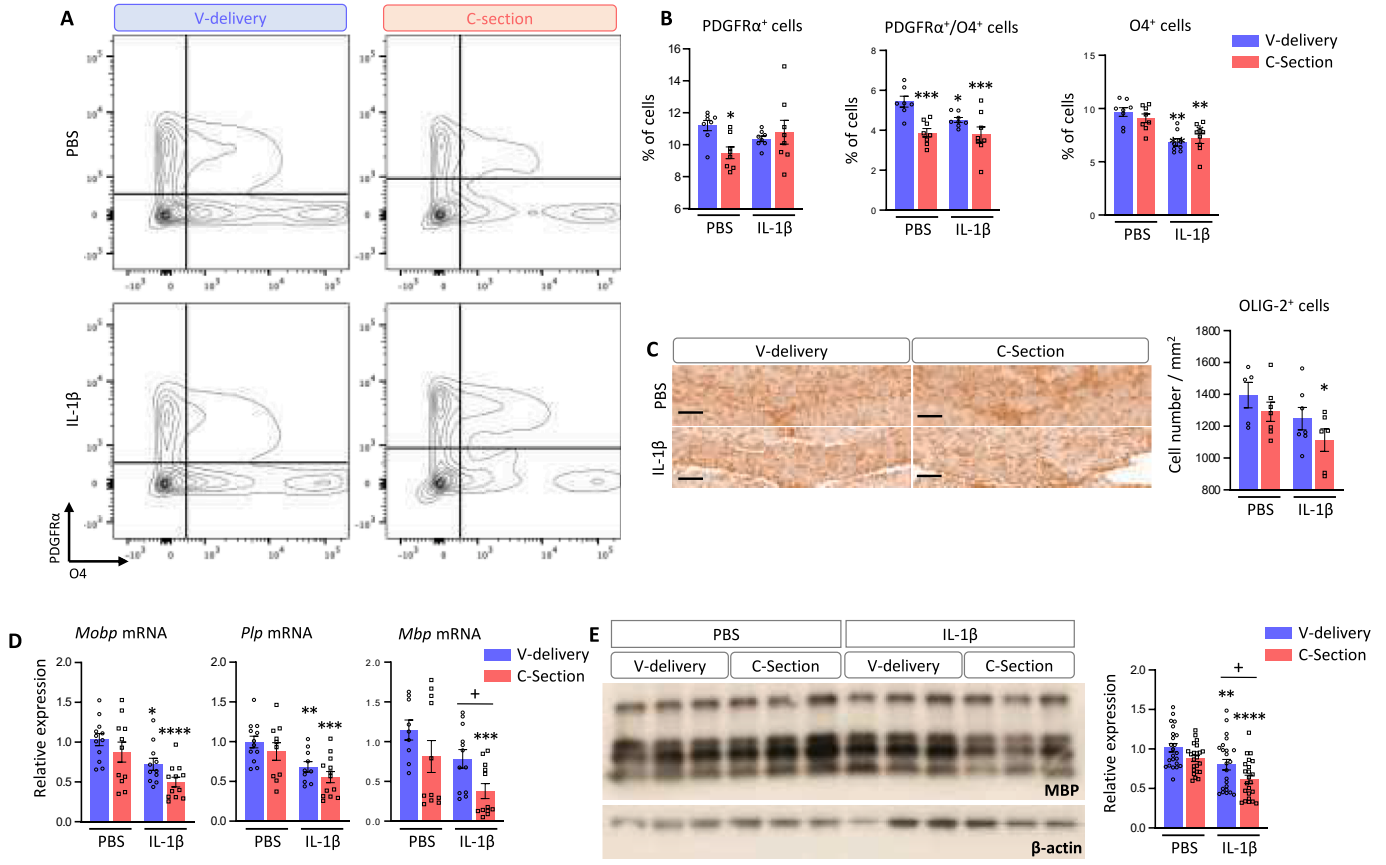

Fig. 3. Impact of IL-1β and C-section on white matter injury. (A-B) Flow cytometry analysis of differentiated oligodendrocyte populations (PDGFRα^{+}/O4^{-}, PDGFRα^{+}/O4^{+}, and PDGFRα^{-}/O4^{+}) in P5 brains from V-delivery ± IL-1β or C-section ± IL-1β mice, n = 4–5 per group, 1 litter per group. (C) Total oligodendrocyte lineage cell density by immuno-histochemistry using OLIG-2 labeling in the corpus callosum of P5 V-delivery ± IL-1β or C-section ± IL-1β mice, n = 5–7 per group, 2 litters per group. Representative images were acquired using a Nanozoomer slide scanner. (D) Relative expression of myelin protein mRNA in P22 anterior brains from V-delivery ± IL-1β or C-section ± IL-1β mice evaluated by qPCR, n = 11–12 per group, 2 litters per group. (E) MBP protein quantification by western blotting for V-delivery ± IL-1β or C-section ± IL-1β brains at P22, n = 23 per group, 3 litters per group. Data are represented as a scatter plot with a bar (mean + SEM). The Kruskal-Wallis test was used followed by an uncorrected Dunn's test. All groups were compared to the V-delivery + PBS group, indicated by *.

2.4. Impact of C-section and systemic inflammation on body weight, behavior, and brain connectivity

Relative to the V-delivery + PBS group, P2 pups in the C-section + PBS group had a significantly higher weight ($p = 0.0481$), while pups in the V-delivery + IL-1β group had a significantly lower weight ($p < 0.0001$). However, the weight of pups in the C-section + IL-1β group was not significantly different (Fig. 4A). We measured weight gain in the animals from birth to early adulthood (8 weeks old, Supplementary Fig.6A/B). Our findings revealed that there was indeed a significant difference in weight gain among the groups. Specifically, both C-section-delivered pups, whether exposed or not to IL-1β, and V-delivery + IL-1β pups exhibited differences in weight gain compared to V-delivery + PBS. Notably, C-section delivery did not exacerbated the effects of IL-1β exposure on weight gain (Supplementary Fig.6B).

Rodents are known to communicate through ultrasonic vocalizations (USVs). Altered perinatal USV emission is a well-described phenotype associated with NDDs (Silverman, 2010). Pups of the C-section + PBS group emitted significantly more calls at P2 than those of the V-delivery + PBS group ($p < 0.0001$; Fig. 4B). The mean frequency of the calls was significantly different in IL-1β groups compared to V-delivery + PBS group.

Similarly, social impairment is often associated with NDDs (Silverman, 2010). We used a previously described early developmental stage social behavioral test based on nest odor affinity to assess social impairment (Morin, 2022; Bokobza, 2022). At P8, pups exposed to perinatal inflammation spent less time on the nest sawdust ($p = 0.014$; Fig. 4C).

In addition, we performed the three-chamber test to evaluate adolescent (6 weeks of age) social interactions (Fig. 4D) (Silverman, 2010). We observed that the V-delivery groups spent significantly more time in the stranger zone than in the object zone ($p = 0.0018$ for PBS and

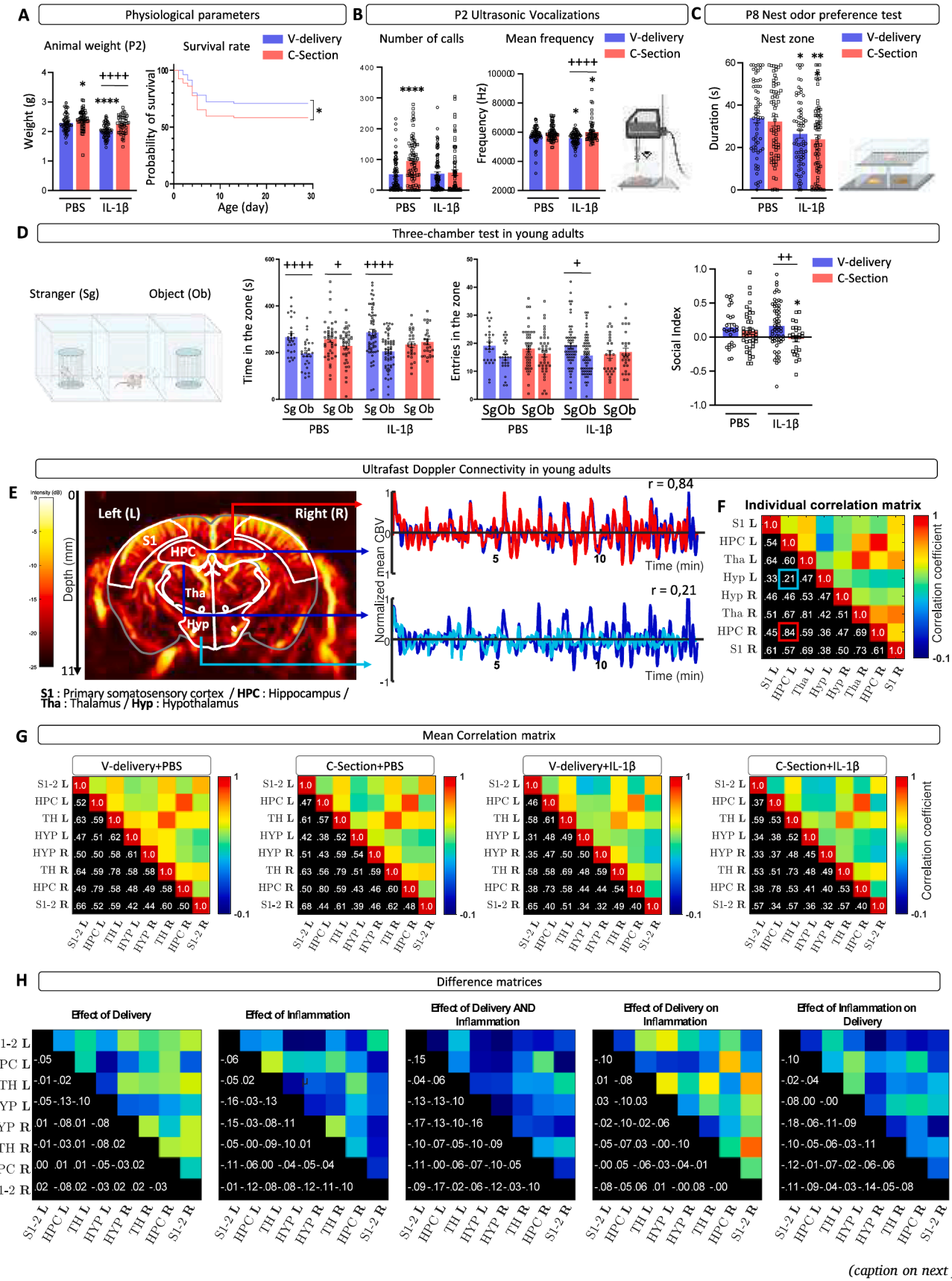

(caption on next page)

Fig. 4. Impact of IL-1β and C-section on weight, behavior, and brain connectivity. (A) Animal weight at P2 and survival rates, n = 28–42 per group, 4–6 litters per group. (B) Ultrasonic vocalization test evaluating total calls emitted by V-delivery ± IL-1β or C-section ± IL-1β animals at P2 in 3 min, n = 28–42 per group, 4–6 litters per group. (C) Nest odor preference test at P8 to evaluate maternal recognition. Results are presented as the mean time spent in the nest zone (3 trials of 1 min/animal), n = 28–42 per group, 4–6 litters per group. (D) Three-chamber test of 5 min at P30-35 comparing V-delivery ± IL-1β or C-section ± IL-1β animals, n = 28–42 per group, 4–6 litters per group. Sg: Stranger and Ob: Unknown object. Data are represented as a scatter plot with a bar (mean + SEM). The Kruskal-Wallis test was used followed by an uncorrected Dunn's test. All groups were compared to the V-delivery + PBS group, indicated by *. (E) Power Doppler image of a mouse brain in the coronal plane with the ROIs overlayed. fUS were acquired using an Iconeus One ultrasound system, which allowed easy registration on the Allen atlas. Mean CBV signals for the ROIs. From each selected ROI, the CBV signals were spatially averaged and temporally processed to obtain a mean CBV signal to compute the pairwise correlation. The correlation between the right and left hippocampus (top) was high (r = 0.84), in contrast to the correlation between the left hippocampus and hypothalamus (down), which was low (r = 0.24). (F) Connectivity matrix. The values in the red and blue boxes correspond to the previous mentioned correlations (resp, L/R HPC, and L HPC/Hyp). (G) Mean correlation matrix of each group of interest. (H) Distribution of the correlation coefficients of the mean matrices of pathological groups. Distribution of the difference between the Z-transformed correlation coefficients of the pathological mean matrices and the V-delivery + PBS matrix. From this distribution, it is assumed that the means of the differences between Z-transformed coefficients are smaller than zero (H1: $\mu<0$). (I) Difference matrices versus the control group. The effect of delivery was tested from the difference of Z-transformed correlation coefficients between the C-section + PBS and V-delivery + PBS groups. The mean of the coefficients of this matrix was significantly smaller than zero ($p < 0.01$, *t*-test). The effect size was measured using Cohen's d (d = 0.20). The same analyses were performed on the difference between the V-delivery + IL-1β and V-delivery + PBS groups for the effect of inflammation ($p < 0.001$, d = 0.65) and on the difference between the C-section + IL-1β and V-delivery + PBS groups for the combined effect of inflammation and delivery ($p < 0.001$, d = 0.79), n = 10–12 per group, 2 litters per group. (For interpretation of the references to color in this figure legend, the reader is referred to the web version of this article.)

$p < 0.0001$ for IL-1β), indicating social interest. However, such social interest was lower in the C-section + PBS group ($p = 0.01$) and not present in the C-section + IL-1β group ($p = 0.598$). We obtained similar results when measuring the number of entries foreach zone: more entries into the stranger zone for the V-delivery groups, which was not observable for the C-section groups. Moreover, C-section + IL-1β animals entered the stranger zone significantly less than V-delivery + PBS animals ($p = 0.016$, Fig. 4D). The C-section + PBS and V-delivery + IL-1β groups had similar social indexes as the V-delivery + PBS group, whereas the C-section + IL-1β group had a significantly lower social index ($p = 0.0472$, Fig. 4D).

Functional ultrasound (fUS) is a recently developed imaging technique, called ultrafast Doppler, to monitor *in vivo* brain activity through fluctuations in cerebral blood volume (CBV) (Deffieux et al., 2021). We averaged the relative fUS signals (which are proportional to CBV) over the pixels of each region of interest before normalization. This resulted in one signal per functional area. We then computed the pairwise correlation of those signals and arranged the correlation coefficients in a connectivity matrix. (Fig. 4E-G). This qualitative (Fig. 4F) and quantitative (Fig. 4H) analysis showed a difference in brain connectivity between PBS-exposed animals born vaginally versus those born via C-section. Specifically, the C-section + PBS group showed less brain connectivity than the V-delivery + PBS group, as indicated by lower-than-zero coefficients in the differential matrix ($p < 0.01$; Fig. 4H-I). This suggests a global reduction in connectivity associated with C-section delivery. We also find lower-to-zero coefficients in the differential matrix between the combined condition group (C-section + IL-1β) and single condition groups (V-delivery + IL-1β $p < 0.05$; C + PBS $p < 0.001$). It suggests an additive effect of C-section over IL-1β exposure. When calculating Cohen's D, we found that the effect of c-section was smaller (D = 0.20, D = 0.18) than the effect of IL-1β (D = 0.65, D = 0.54). Furthermore, fUS revealed an additive effect of C-section with IL-1β exposure, as the combined effect was more significant (D = 0.79) than either condition alone.

3. Discussion

The key finding of the present study is that C-section and systemic neonatal inflammation synergize to exacerbate the deleterious effects of inflammation in a mouse model of EoP. We observed such synergy for the diversity of the gut microbiota, peptidoglycan levels in plasma, microglia/macrophage reactivity, infiltrating monocytes withing the brain associated with a decrease of monocytes in the blood circulation, OLIG-2^+ cell density, myelin gene expression, MBP protein expression, behavior, and, most importantly, brain connectivity. These findings align with the emerging understanding of how early-life interventions and inflammatory states intersect to profoundly influence neurodevelopmental trajectories, identifying bacterial peptidoglycans from the microbiota as potential mediators of the long-term negative consequences on brain development and behavior associated with the combination of C-section and neonatal systemic inflammation.

Previous studies using germ-free (GF) mice and antibiotic-treated animals have revealed the profound effects of gut microbiota on brain development and behavior (Cryan, 2019). Despite ongoing discussions about prenatal microbial exposure in utero, the first major contact with microbes occurs at birth through maternal transmission (Kennedy, 2023). In mammals, one of the key factors impacting early-life gut microbiota composition is the mode of delivery (vaginal vs. C-section). Infants born by C-section often show a reduction in the abundance of beneficial bacteria such as *Bifidobacterium* and *Bacteroides*, which are pivotal for carbohydrate digestion and immune system support (Inchingolo, 2024). Here, we found that intestinal commensal bacteria such as *Streptococcus* spp. and *Enterococcus* spp., which are abundant in the mouse neonate gut of V-delivery + PBS at P5, are significantly affected by C-section and exposure to IL-1β. Notably, these species disappear in the C-section + IL-1β group, indicating clear synergistic effects. Moreover, we discovered that IL-1β, a pro-inflammatory cytokine, promotes the overgrowth of *Corynebacterium* spp. *and Desulfovibrionaceae* spp. in the mouse neonatal gut. Some studies suggest that changes in the abundance of *Corynebacterium spp*., which are opportunistic pathogens, might be associated with dysbiosis (microbial imbalance) in various inflammatory diseases (Haac, 2019). While many *Desulfovibrionaceae* spp. are not typically pathogenic, elevated levels of these sulfate-reducing bacteria have been implicated in inflammatory conditions due to their production of hydrogen sulfide (Kushkevych et al., 2021), which can be toxic to cells and contribute to inflammation. On the other hand, there were specific alterations in the gut microbiota composition in the C-section + PBS group, characterized by an increase in Gram-negative bacteria such as *Escherichia* spp. and *Shigella spp*., both of which can significantly affect intestinal health. Thus, the combination of C-section delivery and neonatal systemic inflammation results in a highly inflammatory microbial environment in the neonatal gut.

Recent studies indicate that bacterial cell components, such as PGN motifs, act as key molecular signals in gut microbiota-host crosstalk in early life (Gonzalez-Santana and Diaz Heijtz, 2020). In the present study, we tested the hypothesis that systemic inflammation leads to enhanced translocation of peptidoglycan fragments into circulation and the developing brain, a process potentially exacerbated by C-section delivery. Intriguingly, plasma peptidoglycan levels were significantly elevated only in the C-section + IL-1β group, while in the brain, we observed a significant reduction in peptidoglycan levels in the V-delivery + IL-1β group. This reduction in brain peptidoglycan levels may be explained by a decrease in the expression of the peptidoglycan transporter PepT1. However, this does not account for the apparent

discrepancy between the elevated systemic peptidoglycan levels in the C-section + IL-1β group and the lack of corresponding changes in the brain. One plausible explanation could be that currently available peptidoglycan ELISA assays are not optimized to detect products from Gram-negative bacteria, such as *meso*-diaminopimelic acid. Instead, these assays primarily detect muramyl-L-alanyl-D-isoglutamine (MDP), the minimal bioactive peptidoglycan motif, and/or the sugar components of peptidoglycan (N-Acetylmuramic Acid and N-Acetylglucosamine) (Arentsen, 2017; Huang, 2019). Nevertheless, the mechanisms governing the translocation of peptidoglycans into the brain remain elusive. It is possible that early-life risk factors, such as C-section and inflammation, might influence this process through both independent and synergistic signaling pathways.

A recent *in vitro* study has identified microglia as primary targets for peptidoglycan fragments originating from the gut microbiota (Spielbauer, 2024). Interestingly, microglia exhibit distinct responses depending on the levels of peptidoglycan fragments such as MDP, with high physiological doses of MDP promoting a pro-inflammatory microglial phenotype (Spielbauer, 2024). Consistent with previous studies, we found that systemic inflammation dramatically increases the gene expression of peptidoglycan-sensing molecules such as *Nod2*, *Pglyrp1,* and *Tlr2* in microglia at P5 in both vaginal delivery and C-section groups. This may be part of the mechanism linking the observed reduction in microbiota diversity with altered microglia/macrophage reactivity, which could have significant consequences for brain development and connectivity. Additionally, oligodendrocyte development and maturation may be influenced by peptidoglycan, as oligodendrocyte precursors express peptidoglycan-sensing molecules such as Nod1 (Gonzalez-Santana and Diaz Heijtz, 2020). This could contribute to the observed reduction in OLIG2 + cell density, changes in myelin-related genes, and altered connectivity. However, further studies are needed to elucidate the specific cellular and signaling pathways that synergize in the context of C-section and inflammation in early life.

The C-section + PBS group showed few alterations, except for diversity of the gut microbiota, the density of PDGFRα$^+$ and PDGFRα$^+$/O4$^+$cells, the number of USV calls, and brain connectivity. In this study, we are demonstrating with isolation induced USVs analysis a short-term effect of C-section and perinatal inflammation on social behavior evaluated. This is supported by studies conducted by Chiesa and collaborators who highlighted a significant increase in the number of calls emitted by C-section born mice (Chiesa et al., 2020; Chiesa, 2021). Additionally, we show a long-term effect of the combined insults on social disinterest. One potential bias in assessing the effects of C-section + PBS was that the present study focused on parameters that we previously showed to be altered in the V-delivery + IL-1β group (Shiow, 2017; Favrais, 2011; Morin, 2022; Bokobza, 2022; Krishnan, 2017; Van Steenwinckel, 2019). Other non-studied parameters could potentially have been altered in the C-section + PBS group.

In conclusion, C-section and systemic inflammation are two significant risk factors for brain maldevelopment that can interact and synergize to exacerbate brain abnormalities. However, this study does not claim causality. If the results of the present study are applicable to human preterm infants; they potentially raise the question of the risk-to-benefit balance of C-section in the context of chorioamnionitis/fusinitis/intra-uterine infection.

4. Materials and Methods

4.1. Animals and models

Experimental protocols were approved by the Ethics committee and the services of the French Ministry in Charge of Higher Education and Research (#10469). Experiments were performed on OF1 strain mice (Charles River, France). C-sections were performed on pregnant mice after cervical dislocation at E19. The surgical procedure was performed under an infrared lamp. Hysterectomy was performed after a combined transverse cutaneous incision of the abdomen and peritoneal incision. Fetuses were extracted from the uterus by manual pressure. Newly born pups were stimulated by massage and transferred to an adoptive mother at the time of the first breathing movements. Surgical procedures lasted between 3- and 5-min. V-delivery occurred spontaneously at E20. Pups from all experimental groups were immediately placed after birth with another OF1 mother that had delivered 24 h earlier. To address concerns about potential confounding effects from the mothers' microbiomes, we made sure not to mix C-section and vaginal delivery pups within the same litter. This precaution was taken because foster mothers have been observed to potentially attack C-section pups due to their perceived weakness. By adopting this approach, we aimed to maintain consistency in the rearing environment while mitigating any potential risks to the pups' well-being.

Like humans with NDD (Bokobza, 2019), there is a strong sex bias in the IL-1β model in which males are more affected than female both in the neuropathology and behavior (unpublished data). Since our goal is to demonstrate a synergic effect, we have decided to focus only on males. Male pups were used for the experiments and injected intraperitoneally (i.p.) twice a day from P1 to P5 with 10 μg/kg IL-1β (Miltenyi Biotec) diluted in 5 μL 1X PBS or with 5 μL 1X PBS alone (Favrais, 2011; Bokobza, 2022; Van Steenwinckel, 2019). Pups were monitored twice a day for any signs of distress according to a clinical score that included feeding, respiratory rate, and weight gain. The variation in sample sizes across experiments is due to the fact that each experiment was performed independently.

4.2. P5 colon collection and bacterial DNA extraction and sequencing

At P5, colons were dissected (from caecum to rectum) and placed at −80 °C. Bacterial DNA was extracted using a QIAamp PowerFecal DNA Kit according to the manufacturer's protocol. The V3-V4 hyper-variable region of the 16S rRNA gene was amplified by PCR using 10 ng of fecal DNA, 0.5 μM primers (Table1), 200 μM dNTP, and 0.5 U DNA-free Taq-polymerase, MolTaq 16S DNA Polymerase (Molzym). The resulting PCR products were purified, quantified, and sequenced using Illumina MiSeq technology (Illumina, CA, USA).

4.3. OTU table generation and statistical analysis

Sequences of the V3-V4 amplicons were processed using the FROGS pipeline to obtain abundance tables of OTUs and their taxonomic affiliation. The successive steps involved de-noising and clustering of the sequences into OTUs using SWARM, chimera removal using VSEARCH, and taxonomic affiliation for each OTU using the RDP Classifier of the SILVA SSU Pintail100 138 database. Statistical analyses were performed using "R" (v.4.0.3). α-diversity analysis was performed using the package phyloseq (v.1.34.0) (McMurdie and Holmes, 2013). For each sample, the observed species and Chao1 index were used to estimate species richness, whereas the Shannon and InvSimpson indexes were used as comprehensive indicators of species diversity and uniformity. Differentially abundant OTUs among the different groups were investigated using DESeq2 (v.1.30.0) by performing the Wald significance test with Benjamini-Hochberg false discovery rate correction. Statistical significance was set at padj < 0.05. Heatmaps were produced using Morpheus software (https://software.broadinstitute.org/morpheus), which is a hierarchical clustering method that couples mean using Pearson's correlation. The cluster annotation can be found in Table 1.

4.4. Protein extraction and peptidoglycan ELISA

Following decapitation at P5, blood collection was performed from the bodies and heads and then the brains were extracted. Plasma was collected after centrifugation for 10 min at 4,000 rpm. Brain proteins were extracted using RIPA Buffer (Sigma-Aldrich) containing protease inhibitors (cOmplete Tablets, Roche) in gentleMACS M tubes using a

gentleMACS dissociator (Miltenyi Biotec) according to the manufacturer's instructions. Samples were centrifuged (10,000 x g, 10 min, 4 °C) and the supernatants stored for later use. ELISA using a mouse peptidoglycan (PG) ELISA Kit (MBS263268, MyBioSource) (Prasad, 2022) was performed following the manufacturer's instructions.

4.5. Western blot

Western blot analysis of MBP was performed on protein lysates from the anterior cerebrum at P22 as previously described (Van Steenwinckel, 2019) using rat anti-MBP (Millipore MAB386 1:500) and anti-β-actin (Sigma- Aldrich AC-74, 1:20,000) for staining.

4.6. Brain dissociation and microglia/macrophage magnetic cell sorting (MACS)

P1 and P5 pups were injected with an overdose of Euthazol and perfused intracardially with 0.9 % NaCl. Brains without the cerebellum and olfactory bulbs were collected and dissociated using a Neural Tissue Dissociation Kit containing papain and a gentleMACS Octo Dissociator with Heater. Magnetic beads coupled with mouse anti-CD11B antibodies (microglia/macrophage) were used for cell isolation according to the manufacturer's protocol (Miltenyi Biotec) as previously described (Favrais, 2011; Bokobza, 2022; Van Steenwinckel, 2019).

4.7. ROS production analysis

$CD11B^+$ cells (80,000) were suspended in Hank's Balanced Salt Solution with Ca^{2+} and Mg^{2+} ($HBSS^{+/+}$) and incubated with luminol (50 μM; Sigma) at 37 °C in the dark for 10 min. Half of the cells were stimulated with phorbol 12-myristate 13-acetate (PMA, Sigma-Aldrich) to enhance basal ROS production as previously described (Morin, 2022; Bokobza, 2021).

4.8. Flow cytometry analyses (FACS)

After dissociation of the brain at P5, as already described, cells were counted using a Nucleocounter (Chemometec). The suspended cells were adjusted to a concentration of 10^7 cells/mL by mixing with FACs buffer (1X Dulbeccos's PBS containing 2 mM EDTA and 0.5 % bovine serum albumin). To limit non-specific binding of antibodies, the cells were incubated for 15 min at 4 °C with an Fc receptor blocker (FVS780, BD Biosciences) according to manufacturer's recommendations. List of all antibodies can be found in Supplementary Table 1. To establish the positivity thresholds for each marker, isotype controls coupled with the same fluorochromes as the specific antibodies were incubated with pools prepared with samples of each group. After 30 min of incubation at 4 °C and in the dark, the cells were washed with FACs buffer, resuspended in PBS, and kept at 4 °C and in the dark until the next morning for flow cytometry analysis (LSR FortessaTM X-20, BD Biosciences). Cell viability, estimated using the FVS780 marker, was greater than 95 %.

Plasma (30 μL) was collected at P5, mixed with 7 μL of EDTA and put on ice. Flow cytometry analysis was performed on 30 μL of total blood/EDTA. Cell viability was assessed with viability marker (Miltenyi) and wash with buffer (95 % PBS 2 mM EDTA pH7.2, 5 % BSA Miltenyi). After centrifugation and removing the supernatant, anti-bodies were added (as report on table 1). Isotype matching fluorochrome-labelled antibodies were used to determine the level of positivity of each marker. 600 μL of FACS lysing solution were added in each tube before centrifugation and 2 washes. Samples were kept overnight in 300 μL of PFA 1 % at 4 °C in the dark before analyses the following day using an LSR FortessaTM X-20 device (BD Biosciences).

Data analyses were performed using FlowJo (v10.10.0). Doublets were excluded based on morphological features, as well as dead cells. Leukocytes were defined as CD45 positive. Within leukocytes population, granulocytes and monocytes were defined as CD11b positive and discriminated by morphological features. Within monocyte population, Ly-6C expression discriminates three subpopulations. Count beads were used to determine absolute cell count. Gating strategies can be found in Supplementary Fig. 5G.

4.9. Multiplex immunoassay (Blood sample)

Plasma (30 μL) was collected from pups at P5, mixed with 7 μL EDTA and put on ice. Using Bio-Plex Pro Mouse Cytokine 23-Plex Immunoassay (#M60009RDPD, Bio-Rad), we quantified 23 cytokines. Assays were performed according to the manufacturer's instructions. Reagents were kept on ice until use, with minimal exposure of the beads to light. All the wash steps were performed on a Bio-Plex Pro Wash Station at room temperature. Data acquisition is done by a Bio-Plex 200 System Reader and Bio-Plex Manager 4.1 software presents data as median fluorescent intensity as well as concentration (pg/ml). Samples with "non-detectable" values are not presented in the histogram.

4.10. RNA extraction and real-time qPCR

Brains for myelin protein gene expression were collected at P22 after cervical dislocation and placed at −80 °C prior to mRNA extraction. mRNA from $CD11B^+$ cells was extracted using an RNA XS Plus extraction kit and that from brains using a NucleoSpin RNA extraction kit according to the manufacturers' protocol (Macherey-Nagel®). Reverse transcription was performed using 350 ng ($CD11B^+$) and 1,000 ng (brain) mRNA with an iScript cDNA synthesis kit (BioRad). Real-time quantitative PCR was performed on triplicate samples using SYBR Green Supermix (BioRad). mRNA levels were calculated using the 2 delta Ct method after normalization against Rpl13a mRNA as the reference mRNA. Expression is expressed as that relative to CD11B + P1 vaginally born/PBS-exposed animals as previously described (Morin, 2022; Van Steenwinckel, 2019; Bokobza, 2021) (Table 2).

4.11. Immunohistochemistry

At P5, brains were processed to paraffin sections by immediate immersion in 4 % formaldehyde for seven days at room temperature prior to dehydration and paraffin embedding. Sections were cut using a microtome. Immunostaining was performed using a Leica Bond max robot and the BOND Polymer Refine Detection kit and mouse antibody to anti-OLIG-2 (18953, Immuno-Biological Laboratories, 1:200). Images were acquired using a Nanozoomer slide scanner (Hamamatsu) and extracted for corpus callosum using QuPath software (Bankhead, 2017).

4.12. Neonatal behavioral tests

Ultrasonic vocalizations were recorded at P2 for 3 min using an ultrasound microphone (Noldus) sensitive to frequencies from 30 to 90 kHz. The pup isolated from the litter was placed in a container (H 4.5 cm x L 10 cm x W 10 cm) inside a soundproof polystyrene box (H 23 cm x L 37 cm x W 24 cm) to avoid interference from external noise. The box temperature was 23.2 degrees. The microphone was placed 10 cm above the pup. Ultrasonic vocalizations were recorded using Ultravox XT3.1 software (Noldus) and analyzed using the https://usv.pasteur.cloud tool (de Chaumont, 2021).

Social behavior at P8 was evaluated by the nest odor preference test as previously described (Bokobza, 2022). The room temperature was 24 °C. The test apparatus (L 20 cm x W 13 cm) was composed of three zones: a nest zone, with the nest, and a clean zone, with clean sawdust (L 7 cm x W 13 cm), separated by a neutral zone (L 6 cm x W 13 cm) without sawdust. Over the three zones, a grid was placed for the pup to walk on. The pup isolated from the litter was placed on top of the neutral zone at the beginning of the test and the time spent in each area measured for 1 min. Representation is the mean duration of the three 1-min trials. The test apparatus was cleaned with 70 % ethanol between

Table 2
Qpcr primers sequences.

Gene	Target protein and abbreviation	Forward	Reverse
Rpl13a	Ribosomal protein L13 a	ACA GCC ACT CTG GAG GAG AA	GAG TCC GTT GGT CTT GAG GA
Ptgs2	Prostaglandin-Endoperoxide Synthase 2 (=Cox2)	TCA TTC ACC AGA CAG ATT GCT	AAG CGT TTG CGG TAC TCA TT
Tnf	Tumor necrosis factor	GCC TCT TCT CAT TCC TGC TT	AGG GTC TGG GCC ATA GAA CT
Il1ra	Interleukin 1 receptor antagonist	TTG TGC CAA GTC TGG AGA TG	TTC TCA GAG CGG ATG AAG GT
Il4ra	Interleukin 4 receptor alpha	GGA TAA GCA GAC CCG AAG C	ACT CTG GAG AGA CTT GGT TGG
Socs3	Suppressor of cytokines 3	CGT TGA CAG TCT TCC GAC AA	TAT TCT GGG GGC GAG AAG AT
Mog	Myelin-oligodendrocyte glycoprotein	AAG AGG CAG CAA TGG AGT TG	GAC CTG CAG GAG GAT
Plp	Proteolipid protein	CCA AAT GAC CTT CCA CCT GT	CGA AGT TGT AAG TGG CAG CA
Mobp	Myelin- Associated Oligodendrocyte Basic Protein	TCCACAGGAACC TTTCACAA	TCCTTGGCCATTTTC TGACT
Cd32	Cluster Differenciation 32	CTG GAA GAA GCT GCC AAA AC	CCA ATG CCA AGG GAG ACT AA
Arg1	Arginase 1	GTG AAG AAC CCA CGG TCT GT	GCC AGA GAT GCT TCC AAC TG
Nod2	nucleotide- binding oligomerization domain 2	GAACTCTGCCTAGAGGAAAACCA	GATGCCATTGTTGGACAGTTTCA
Pglyrp1	Peptidoglycan Recognition Protein 1	TGTTGTTTGCCTGTGCTCTC	GATCACCACGTAGCGAACTG
Tlr2	Toll-like receptor 2	CTCCCACTTCAGGCTCTTTG	ACCCAAAACACTTCCTGCTG
ARNr 16S		CTTTCCCTACACGACGCTCTTCCG ATCTACGGRAGGCWGCAG	GGAGTTCAGACGTGTGCTCTTCC GATCTTACCAGGGTATCTAATCCT

pups.

4.13. Adolescent behavioral tests

At six weeks, a three-chamber social and behavioral test was conducted on the mice. The experiment involved placing the mouse in a three-chamber box with openings between the chambers. The test was performed in two sessions. During the first session, the mouse was allowed to freely explore the empty apparatus for 10 min. The following day, the mouse was placed in the middle chamber while a stranger mouse was placed in one of the chambers (either left or right) and an object placed in the other chamber. The mouse being tested was allowed to freely move around the entire apparatus for 10 min. The experiments were recorded and analyzed using Any-Maze software. The analysis was based on the time spent in each chamber and the number of entries made. The social Index was calculated as follows:

$$SocialIndex = \frac{TimewithStranger - TimewithObject}{(TimewithStranger + TimewithObject)}$$

4.14. Ultrafast Doppler acquisition

At six weeks, animals (N = 38) were anesthetized with a blend of ketamine (75 mg/kg) and xylazine (15 mg/kg) per animal. A craniotomy was performed after fixing their head in a stereotaxic frame. Functional ultrasound images were acquired at a frame rate of 2.5 Hz using an Iconeus One ultrasound system (Iconeus, Paris, France) with an Ico-Prime linear ultrasound probe (15 MHz, 128 elements, pitch 0.11 mm). The probe was placed at the coronal plane showing the somatosensory cortex, thalamus, hypothalamus, and hippocampus. Detailed explanations for atlas registration and brain positioning can be found in (Bertolo, 2021; Nouhoum, 2021). fUS images were recorded for 15 min with a field-of-view that was 14 mm wide and 11 mm deep. Recordings from animals presenting with a hemorrhage, stroke, or spreading depression resulting from surgical procedures were excluded from the analysis. It represents 11 animals, no differences between groups were visible. Epochs with motion or other artifacts were also removed for each animal during data processing. Finally, the fUS signal for each pixel (proportional to CBV) was filtered using a bandpass filter (4th order Butterworth) with frequency cut-offs of 0.01 and 0.1 Hz and transformed as a relative value (%) to the average.

We calculated the mean matrices for each animal to compare connectivity patterns between conditions. To ensure that the values were normally distributed after transformation, we performed a Z-Fisher transformation of the correlation coefficient. Then, we subtracted the mean matrix of the control group (vaginally born/PBS-exposed animals) from the mean matrix of each other condition. We also subtracted the group with combined conditions (C-section + IL-1β) from each group with a single condition (V-delivery + IL-1β animals and C-section + PBS animals). We hypothesized that the "difference coefficients" would be, on average, negative, which we tested using a one-tail *t*-test on the coefficient of the matrices of differences (H1 hypothesis: difference coefficient < 0). We applied a Bonferroni-Holm correction for multiple comparisons. For a more quantitative understanding of the modification of connectivity of each condition, we computed Cohen's d, which measures the effect size (typical values: d = 0.2 means small effect, d = 0.5 medium effect, d = 0.8 large effect).

4.15. Statistical analysis

Data are expressed as mean values with the standard error of the mean (SEM). GraphPad Prism Software was used for all statistical analysis. Outliers were removed applying ROUT test at Q = 2 %. Multiple comparisons for the same data set were performed by one-way analysis of variance (ANOVA) using the Kruskal-Wallis test followed by an uncorrected Dunn's test or two-way ANOVA followed by a Šídák's multiple comparisons post-hoc test in comparison to the V-delivery + PBS group.

Author Contributions:

CM, FF, VF, JH, LS, RM, CD, RDH, BF, BM, SA, MT, JVS, PG, and CB: study concept and design. CM, FF, JM, DG, AHO, IS, SD, VF, JP, LT, JH, LS, AM, RM, ML, CD, ADD, RDH, BF, BM, SA, MT, JSV, PG, and CB: data acquisition and analysis. CM, FF, VF, JH, AM, CD, ADD, RDH, BF, BM, SA, MT, JVS, PG, and CB: drafting of the text and figures.

CRediT authorship contribution statement

Cécile Morin: Writing – review & editing, Writing – original draft, Methodology, Formal analysis, Data curation, Conceptualization. **Flora Faure:** Writing – review & editing, Writing – original draft, Formal analysis, Data curation, Conceptualization. **Julie Mollet:** Writing – review & editing, Formal analysis. **David Guenoun:** Visualization, Formal analysis, Data curation. **Ariane Heydari-Olya:** Formal analysis, Data curation. **Irvin Sautet:** Formal analysis, Data curation. **Sihao Diao:** Formal analysis, Data curation. **Valérie Faivre:** Methodology, Formal analysis, Data curation, Conceptualization. **Julien Pansiot:** Formal analysis, Data curation. **Lara Tabet:** Data curation. **Jennifer Hua:** Methodology, Formal analysis, Data curation. **Leslie Schwendimann:** Methodology, Formal analysis, Data curation. **Amazigh Mokhtari:**

Visualization, Formal analysis, Data curation. **Rebeca Martin-Rosique:** Writing – review & editing, Writing – original draft, Methodology, Investigation, Formal analysis, Data curation. **Sead Chadi:** Formal analysis, Data curation. **Mireille Laforge:** Supervision. **Charlie Demené:** Writing – review & editing, Writing – original draft, Supervision, Funding acquisition, Formal analysis, Conceptualization. **Andrée Delahaye-Duriez:** Writing – review & editing, Writing – original draft, Supervision, Funding acquisition, Formal analysis. **Rochellys Diaz-Heijtz:** Writing – review & editing, Writing – original draft, Investigation, Funding acquisition, Formal analysis. **Bobbi Fleiss:** Writing – original draft, Visualization, Funding acquisition, Formal analysis, Data curation. **Boris Matrot:** Writing – original draft, Methodology, Formal analysis. **Sandrine Auger:** Writing – original draft, Formal analysis, Data curation. **Mickael Tanter:** Writing – original draft, Visualization, Investigation, Funding acquisition, Conceptualization. **Juliette Van Steenwinckel:** Writing – review & editing, Writing – original draft, Supervision, Investigation, Funding acquisition, Formal analysis, Data curation, Conceptualization. **Pierre Gressens:** Writing – review & editing, Writing – original draft, Visualization, Validation, Supervision, Resources, Project administration, Investigation, Funding acquisition, Conceptualization. **Cindy Bokobza:** Writing – review & editing, Writing – original draft, Visualization, Supervision, Project administration, Investigation, Funding acquisition, Formal analysis, Data curation, Conceptualization.

Declaration of Competing Interest

The authors declare that they have no known competing financial interests or personal relationships that could have appeared to influence the work reported in this paper.

Acknowledgments

Schematic representations were created using BioRender App. PG acknowledges support from Inserm, the Université Paris Cité, Fondation Grace de Monaco, Inserm International Research Project “IntegrA”, French “Investissement d’Avenir- ANR-11-INBS-0011 NeurATRIS” and ANR-23-IAHU-0010 (France 2030). JVS acknowledges support from the Agence Nationale de la Recherche ANR-22-CE14-0051-02, CB acknowledges support from “Investissement d’Avenir- ANR-17-EURE-001-EUR G.E.N.E.’’ and the ANR (contract ANR-22-CE37-0019). BM acknowledges support from Inserm, the Université Paris Cité, Fondation Air Liquide, Fédération pour la Recherche sur le Cerveau, and the Région Ile-de-France. RDH acknowledges support from the Swedish Research Council (2018-06232). BF acknowledges support from the Cerebral Palsy Alliance, Australia. SA acknowledges support from INRAE. ADD acknowledges support from the Université Sorbonne Paris Nord and the French National Research Agency (#ANR-18-CE17-0009-01, #ANR-18-CE37-0002- 03, #ANR-21-RHUS-009). MT acknowledges support from the Inserm Accelerator of Technological Research on Biomedical Ultrasound. JVS and ML acknowledges support from Fondation de France. PG, FF, BF, MT, and CB acknowledge support from the European Union’s Horizon 2020 Research and Innovation program under Grant Agreement No 874721 PREMSTEM. The supporting bodies played no role in any aspect of study design, analysis, interpretation, or the decision to publish this data.

Appendix A. Supplementary data

Supplementary data to this article can be found online at https://doi.org/10.1016/j.bbi.2024.10.023.

Data availability

Data will be made available on request.

References

Arentsen, T., et al., 2017. The bacterial peptidoglycan-sensing molecule Pglyrp2 modulates brain development and behavior. Mol. Psychiatry 22 (2), 257–266.
Arentsen, T., et al., 2018. Sex-dependent alterations in motor and anxiety-like behavior of aged bacterial peptidoglycan sensing molecule 2 knockout mice. Brain Behav. Immun. 67, 345–354.
Backhed, F., et al., 2015. Dynamics and Stabilization of the Human Gut Microbiome during the First Year of Life. Cell Host Microbe 17 (5), 690–703.
Ball, G., et al., 2013. The influence of preterm birth on the developing thalamocortical connectome. Cortex 49 (6), 1711–1721.
Ball, G., et al., 2015. Thalamocortical Connectivity Predicts Cognition in Children Born Preterm. Cereb. Cortex 25 (11), 4310–4318.
Bankhead, P., et al., 2017. QuPath: Open source software for digital pathology image analysis. Sci. Rep. 7 (1), 16878.
Beli, E., et al., 2018. Restructuring of the gut microbiome by intermittent fasting prevents retinopathy and prolongs survival in db/db mice. Diabetes 67 (9), 1867–1879.
Bennet, L., et al., 2018. Chronic inflammation and impaired development of the preterm brain. J. Reprod. Immunol. 125, 45–55.
Bertolo, A., et al., 2021. Whole-Brain 3D Activation and Functional Connectivity Mapping in Mice using Transcranial Functional Ultrasound Imaging. J. Vis. Exp. 168.
Boggs, J.M., 2006. Myelin basic protein: a multifunctional protein. Cell. Mol. Life Sci. 63 (17), 1945–1961.
Bokobza, C., et al., 2019. Neuroinflammation in preterm babies and autism spectrum disorders. Pediatr. Res. 85 (2), 155–165.
Bokobza, C., et al., 2021. miR-146b protects the perinatal brain against microglia-induced hypomyelination. Ann. Neurol.
Bokobza, C., et al., 2022. miR-146b Protects the Perinatal Brain against Microglia-Induced Hypomyelination. Ann. Neurol. 91 (1), 48–65.
Bokobza, C., et al., 2022. Targeting the brain 5-HT7 receptor to prevent hypomyelination in a rodent model of perinatal white matter injuries. J. Neural Transm. (Vienna).
Buser, J.R., et al., 2012. Arrested preoligodendrocyte maturation contributes to myelination failure in premature infants. Ann. Neurol. 71 (1), 93–109.
Chevallier, M., et al., 2022. Mortality and significant neurosensory impairment in preterm infants: an international comparison. Arch Dis Child Fetal Neonatal Ed 107 (3), 317–323.
Chiesa, M., et al., 2021. Brain Volumes in Mice are Smaller at Birth After Term or Preterm Cesarean Section Delivery. Cereb. Cortex 31 (8), 3579–3591.
Chiesa, M., Ferrari, D.C., Ben-Ari, Y., 2020. Alteration in the time and/or mode of delivery differentially modulates early development in mice. Mol. Brain 13 (1), 34.
Cryan, J.F., et al., 2019. The Microbiota-Gut-Brain Axis. Physiol. Rev. 99 (4), 1877–2013.
Curran, E.A., et al., 2015. Research review: Birth by caesarean section and development of autism spectrum disorder and attention-deficit/hyperactivity disorder: a systematic review and meta-analysis. J Child Psychol. Psychiatry 56 (5), 500–508.
Dahl, C., et al., 2018. Preterm infants have distinct microbiomes not explained by mode of delivery, breastfeeding duration or antibiotic exposure. Int. J. Epidemiol. 47 (5), 1658–1669.
de Chaumont, F., et al., 2021. LMT USV Toolbox, a Novel Methodological Approach to Place Mouse Ultrasonic Vocalizations in Their Behavioral Contexts-A Study in Female and Male C57BL/6J Mice and in Shank3 Mutant Females. Front. Behav. Neurosci. 15, 735920.
Deffieux, T., Demene, C., Tanter, M., 2021. Functional Ultrasound Imaging: A New Imaging Modality for Neuroscience. Neuroscience 474, 110–121.
Favrais, G., et al., 2011. Systemic inflammation disrupts the developmental program of white matter. Ann. Neurol. 70 (4), 550–565.
Gonzalez-Santana, A., Diaz Heijtz, R., 2020. Bacterial Peptidoglycans from Microbiota in Neurodevelopment and Behavior. Trends Mol. Med. 26 (8), 729–743.
Haac, B.E., et al., 2019. A Distinct Gut Microbiota Exists Within Crohn’s Disease-Related Perianal Fistulae. J. Surg. Res. 242, 118–128.
Hagberg, H., Peebles, D., Mallard, C., 2002. Models of white matter injury: comparison of infectious, hypoxic-ischemic, and excitotoxic insults. Ment. Retard. Dev. Disabil. Res. Rev. 8 (1), 30–38.
Huang, K., et al., 2019. Elective caesarean delivery and offspring’s cognitive impairment: Implications of methylation alteration in hippocampus glucocorticoid signaling genes. Brain Res. Bull. 144, 108–121.
Iglesias-Vazquez, L., et al., 2020. Composition of Gut Microbiota in Children with Autism Spectrum Disorder: A Systematic Review and Meta-Analysis. Nutrients 12 (3).
Inchingolo, F., et al., 2024. The Impact of Cesarean Section Delivery on Intestinal Microbiota: Mechanisms, Consequences, and Perspectives-A Systematic Review. Int. J. Mol. Sci. 25 (2).
Kennedy, K.M., et al., 2023. Questioning the fetal microbiome illustrates pitfalls of low-biomass microbial studies. Nature 613 (7945), 639–649.
Koenig, J.E., et al., 2011. Succession of microbial consortia in the developing infant gut microbiome. PNAS 108 (Suppl 1), 4578–4585.
Korpela, K., et al., 2018. Intestinal microbiota development and gestational age in preterm neonates. Sci. Rep. 8 (1), 2453.
Krishnan, M.L., et al., 2017. Integrative genomics of microglia implicates DLG4 (PSD95) in the white matter development of preterm infants. Nat. Commun. 8 (1), 428.
Kushkevych, I., Dordevic, D., Vitezova, M., 2021. Possible synergy effect of hydrogen sulfide and acetate produced by sulfate-reducing bacteria on inflammatory bowel disease development. J. Adv. Res. 27, 71–78.
Leviton, A., Dammann, O., 2004. Coagulation, inflammation, and the risk of neonatal white matter damage. Pediatr. Res. 55 (4), 541–545.
McMurdie, P.J., Holmes, S., 2013. phyloseq: an R package for reproducible interactive analysis and graphics of microbiome census data. PLoS One 8 (4), e61217.

Morin, C., et al., 2022. The Impact of Mouse Preterm Birth Induction by RU-486 on Microglial Activation and Subsequent Hypomyelination. Int. J. Mol. Sci. 23 (9).
Nadeau, H.C., Subramaniam, A., Andrews, W.W., 2016. Infection and preterm birth. Semin. Fetal Neonatal Med. 21 (2), 100–105.
Nouhoum, M., et al., 2021. A functional ultrasound brain GPS for automatic vascular-based neuronavigation. Sci. Rep. 11 (1), 15197.
O'Reilly, H., et al., 2021. Extremely preterm birth and autistic traits in young adulthood: the EPICure study. Mol Autism 12 (1), 30.
Prasad, R., et al., 2022. Microbial Signatures in The Rodent Eyes With Retinal Dysfunction and Diabetic Retinopathy. Invest. Ophthalmol. Vis. Sci. 63 (1), 5.
Rangon, C.M., et al., 2018. Myelination induction by a histamine H3 receptor antagonist in a mouse model of preterm white matter injury. Brain Behav. Immun. 74, 265–276.
Rao, C., et al., 2021. Multi-kingdom ecological drivers of microbiota assembly in preterm infants. Nature 591 (7851), 633–638.
Royet, J., Gupta, D., Dziarski, R., 2011. Peptidoglycan recognition proteins: modulators of the microbiome and inflammation. Nat. Rev. Immunol. 11 (12), 837–851.
Shiow, L.R., et al., 2017. Reactive astrocyte COX2-PGE2 production inhibits oligodendrocyte maturation in neonatal white matter injury. Glia 65 (12), 2024–2037.
Silverman, J.L., et al., 2010. Behavioural phenotyping assays for mouse models of autism. Nat. Rev. Neurosci. 11 (7), 490–502.
Spielbauer, J., et al., 2024. Bacterial peptidoglycan signalling in microglia: Activation by MDP via the NF-kappaB/MAPK pathway. Brain Behav. Immun. 121, 43–55.
Stolp, H.B., et al., 2019. Interneuron Development Is Disrupted in Preterm Brains With Diffuse White Matter Injury: Observations in Mouse and Human. Front. Physiol. 10, 955.
Thanh, B.Y.L., et al., 2019. Mode of delivery and pregnancy outcomes in preterm birth: a secondary analysis of the WHO Global and Multi-country Surveys. Sci. Rep. 9 (1), 15556.
Thion, M.S., et al., 2018. Microbiome Influences Prenatal and Adult Microglia in a Sex-Specific Manner. Cell 172 (3), 500–516 e16.
Tosoni, G., Conti, M., Diaz Heijtz, R., 2019. Bacterial peptidoglycans as novel signaling molecules from microbiota to brain. Curr. Opin. Pharmacol. 48, 107–113.
Twilhaar, E.S., et al., 2022. Profiles of Functioning in 5.5-Year-Old Very Preterm Born Children in France: The EPIPAGE-2 Study. J. Am. Acad. Child Adolesc. Psychiatry 61 (7), 881–891.
Underwood, M.A., Sohn, K., 2017. The Microbiota of the Extremely Preterm Infant. Clin. Perinatol. 44 (2), 407–427.
Van Steenwinckel, J., et al., 2019. Decreased microglial Wnt/beta-catenin signalling drives microglial pro-inflammatory activation in the developing brain. Brain 142 (12), 3806–3833.
Veerasammy, S., et al., 2020. Perinatal IL-1beta-induced inflammation suppresses Tbr2(+) intermediate progenitor cell proliferation in the developing hippocampus accompanied by long-term behavioral deficits. Brain Behav Immun Health 7, 100106.
Verney, C., et al., 2010. Neuronal damage in the preterm baboon: impact of the mode of ventilatory support. J. Neuropathol. Exp. Neurol. 69 (5), 473–482.
Vogel, J.P., et al., 2015. New WHO recommendations to improve the outcomes of preterm birth. Lancet Glob. Health 3 (10), e589–e590.
Wu, J., et al., 2022. Peptidoglycan-mediated bone marrow autonomic neuropathy impairs hematopoietic stem/progenitor cells via a NOD1-dependent pathway in db/db mice. Stem Cells Int. 2022.
Xiao, L., et al., 2021. Deterministic transition of enterotypes shapes the infant gut microbiome at an early age. Genome Biol. 22 (1), 243.
Yip, B.H.K., et al., 2017. Caesarean section and risk of autism across gestational age: a multi-national cohort study of 5 million births. Int. J. Epidemiol. 46 (2), 429–439.
Zuffa, S., et al., 2023. Early-life differences in the gut microbiota composition and functionality of infants at elevated likelihood of developing autism spectrum disorder. Transl. Psychiatry 13 (1), 257.